J Mater Sci (2010) 45:5191–5195
DOI 10.1007/s10853-010-4556-7

Master sintering curve applied to the Field-Assisted Sintering Technique

Olivier Guillon · Jochen Langer

Received: 5 February 2010 / Accepted: 16 April 2010 / Published online: 6 May 2010

Abstract The master sintering curve approach was extended theoretically to the Field-Assisted Sintering Technique (or SPS). Experimental data from constant heating rate testing confirm the general applicability of this framework. An apparent activation energy of ~290 kJ/mol was found for ultrafine alumina below 1200 °C. As alumina densifies by grain boundary diffusion in the present conditions, this low value of the apparent activation energy might be due to thermal gradients in the specimens induced by rapid heating.

Introduction

The master sintering curve (MSC) approach has been derived by Johnson and co-workers [1–3] for free sintering from a simplified model involving both volume and grain boundary diffusion. The normalized densification rate is given by:

$$\frac{\mathrm{d}\rho}{\rho \mathrm{d}t} = \frac{3\gamma\Omega}{kT}\left(\frac{\Gamma_{\mathrm{V}} D_{\mathrm{V}}}{G^3} + \frac{\Gamma_{\mathrm{b}} D_{\mathrm{b}}}{G^4}\right), \quad (1)$$

where ρ is the density, t the time, γ the surface energy, Ω is the atomic volume, k is the Boltzmann constant, T the absolute temperature, D_{v} and D_{b} the coefficients for lattice and grain boundary diffusion, respectively, Γ_{V} and Γ_{b} scaling parameters also depending on density, and G the mean grain diameter. By separating terms related to temperature from all others, it is possible by integrating over time to define the function Θ:

$$\Theta(t, T(t)) \equiv \int_0^t \frac{1}{T}\exp\left(\frac{-Q}{RT}\right)\mathrm{d}t = \frac{k}{\gamma\Omega D_0}\int_{\rho_0}^{\rho}\frac{G(\rho)^m}{3\rho\Gamma(\rho)}, \quad (2)$$

where Q is the apparent activation energy for sintering, R the gas constant, D_0 is the pre-exponential term for the diffusion coefficient, m grain size exponent is 3 or 4 for volume or grain boundary diffusion, respectively. $\Theta(t, T(t))$ is only a function of thermal history. The plot of density ρ versus Θ is defined as the MSC, which can be fit using a sigmoidal function [3]. In case of more complex shape, the MSC can be approximated piecewise [4]. A unique MSC can be obtained if only one diffusion mechanism is dominant during sintering and the microstructure is function only of density. Usually, constant heating rate experiments are carried out for a given specimen type (raw powder and processing parameters should be kept identical) and the activation energy can be found from optimizing the mean square residual between all curves [3, 5–7]. As the effect of surface diffusion is neglected in the model, relatively large discrepancies can be observed between apparent activation energy values and expected values characterizing for example grain boundary diffusion process, especially when low-heating rate or low-temperature schedules are chosen [3, 8]. Similar approach involving isodensity or isostrain lines (in case of anisotropic shrinkage) was used to empirically fit the densification behavior of alumina samples [9]. Alternatively, MSCs can also be obtained from other constitutive models, including continuum mechanical ones [10].

The effect of an applied load during hot pressing (HP) has been further taken into account by An and Johnson, leading to 3D maps including pressure [11] and was successfully applied to alumina. Experiments were conducted at a given heating rate (10 °C/min) and apparent constant

O. Guillon (✉) · J. Langer
Technische Universität Darmstadt, Institute of Materials Science, Petersenstr. 23, 64287 Darmstadt, Germany
e-mail: guillon@ceramics.tu-darmstadt.de

pressures of 6.9–34.5 MPa were used. Here, we propose to develop equations for the Field-Assisted Sintering Technique (FAST, also known as SPS, Spark Plasma Sintering [12]) as function of the heating rate. This technique, which presents large similarities with HP, enables the manufacturing of dense [13] and transparent [14] ceramics as well as nanocrystalline metals [15]. It enjoys a rapid development and enables the use of a large range of heating rates (up to several hundreds of degrees per minute). A series of constant heating rate experiments complements this theoretical framework and validates the present approach.

Theoretical framework

During HP and FAST, a uniaxial mechanical load is applied so that lateral shrinkage of the sample remains negligible. Under the assumption that (i) moderate loads are applied (i.e., small enough not to activate plasticity), but larger than the sintering stress (which is true if the strain rate under load is large compared to the free sintering rate) and (ii) deformation is controlled by a diffusional process (assumptions validated for alumina by Coble and Ellis [16]), the densification rate, equal to the axial strain rate, can be described by the following general equation [17]:

$$\frac{1}{\rho}\frac{\mathrm{d}\rho}{\mathrm{d}t} = \frac{HD}{G^m kT}(\varphi p_\mathrm{a})^n, \tag{3}$$

where H a numerical constant, $D = D_0 \exp\left(\frac{-Q}{RT}\right)$ is the diffusion coefficient of the rate-controlling species, D_0 is a pre-exponential factor, φ is the stress intensification factor which is a function of porosity, p_a is the uniaxial applied stress and the so-called stress exponent n depend on the mechanism of densification ($n = 1$ for grain boundary, lattice diffusion, or viscous flow). The normalized densification rate $\frac{1}{\rho}\frac{\mathrm{d}\rho}{\mathrm{d}t}$ is now equal to the opposite of vertical strain rate $-\frac{\mathrm{d}\varepsilon_z}{\mathrm{d}t}$ as no radial shrinkage takes place. The stress intensification factor describes how the macroscopic-applied stress is magnified at the microscopic scale and depends here only on density. It is also possible here to further separate the variables and to get the following equation:

$$\frac{kG^m}{\rho H D_0 p_\mathrm{a}^n \varphi^n}\mathrm{d}\rho = \frac{1}{T}\exp\left(-\frac{Q}{RT}\right)\mathrm{d}t \tag{4}$$

After integration,

$$\frac{k}{HD_0 p_\mathrm{a}^n}\int_{\rho_0}^{\rho}\frac{G^m}{\rho\varphi^n}\mathrm{d}\rho = \int_0^t \frac{1}{T}\exp\left(-\frac{Q}{RT}\right)\mathrm{d}t \equiv \Theta(t,T) \tag{5}$$

which allows us to use the classical methodology of MSC as in the free sintering case, provided the applied stress p_a is constant. As in the free sintering case, the effect of surface diffusion is neglected in the present treatment of the MSC. Nevertheless, surface diffusion could play a role during sintering by FAST, particularly when particle sliding or grain boundary sliding takes place.

Experimental procedure

All experiments were made with the same FAST equipment (HP D 25/1, FCT Systeme, Germany). The powder used is an ultrafine α-Al_2O_3 (purity of 99.99% and median particle size of 150 nm; TMDAR, Taimei Chem., Tokyo, Japan). Raw powder was sieved through a 100 μm mesh, allowing better packing and reproducibility of the green bodies. The interior of the graphite die and the surfaces of the punches were covered by a compressible graphite foil to maximize the contact area between the rough powder compact surface and the punches and reduce friction as well as temperature gradients. Moreover, the exterior of the die was covered by graphite felt with a thickness of $\sim$10 mm to reduce temperature gradients. The initial sample height was $\sim$11 mm with a relative green density of 55 ± 2% (measured geometrically). Various heating rates from 35 to 150 K min^{-1} were used up to a temperature of 1200 °C under vacuum. Isothermal step at the maximum temperature lasted 10 min. A pulse pattern of 25:5 was adopted for heating. A load of 15.7 kN, corresponding to 50 ± 1.6 MPa, was kept constant. Axial shrinkage was measured with a resolution of 10 μm and the thermal expansion of the machine was taken into account for every heating rate through reference measurements obtained by placing a dense alumina sample in the pressing tool and subtracting these measured values from the original sintering curves. Data points were recorded every 1 s. The temperature was measured with an axial pyrometer, and calibrated with melting copper [18]. The densities of all sintered specimens were measured by the Archimedes method in water at room temperature.

Results and discussion

Figure 1 plots the relative density as function of time for the different heating rates, starting from 800 °C, temperature at which hardly any densification has taken place and including the isothermal step (reference for the time scale). As expected, specimens sintered at a lower heating rate have a higher density when reaching the isothermal step, but all samples are fully sintered at the end of the holding time (relative density $\sim$99%). Furthermore, the strain rates measured under applied load are significantly larger than in the free sintering case, which valids the assumption for using Eq. 3. For example, the densification rate of TMDAR

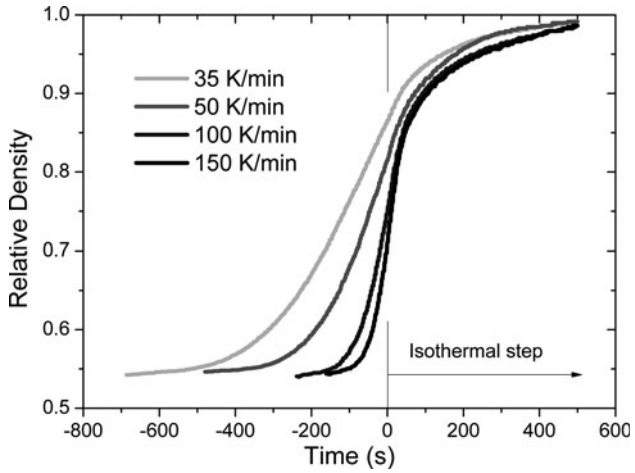

Fig. 1 Relative density curves as a function of time for different heating rates: 35, 50, 100, 150 K/min (from 800 to 1200 °C, under a constant applied stress of 50 MPa). Time origin represents the beginning of the isothermal step

dry pressed specimens freely sintered is almost zero at 1200 °C reached by heating at a rate of 30 K/min and a density of 86% [19]. This density is reached at the beginning of the isothermal time with a heating rate of 35 K/min in the FAST setup, where still significant densification occurs.

Figure 2 shows the relative density now as function of Log(Θ), which is the so-called MSC. For higher values of Log(Θ), i.e., at the end of the sintering cycle, the curve is not tangent to the horizontal full density line as typically observed for free sintering, because densification rate is still large. This feature can also be observed on An and Johnson's curves from HP investigations [11]. Longer isothermal times should simply be required to get a full classical sigmoidal shape. The value of the activation

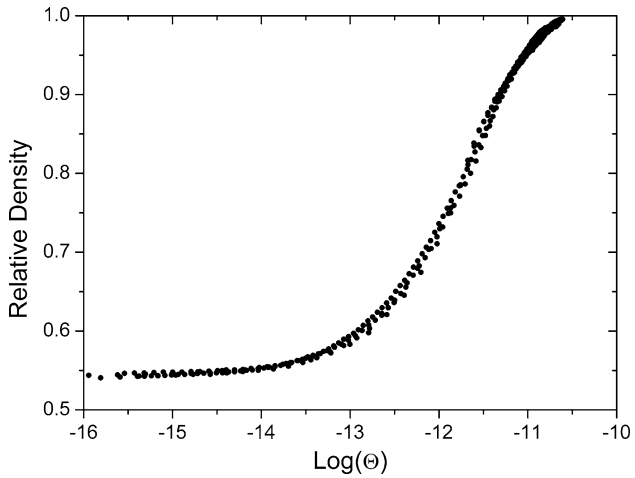

Fig. 2 Master sintering curve (relative density as a function of Log (Θ)) for all heating rates, including the isothermal step, with an apparent activation energy of 290 kJ/mol

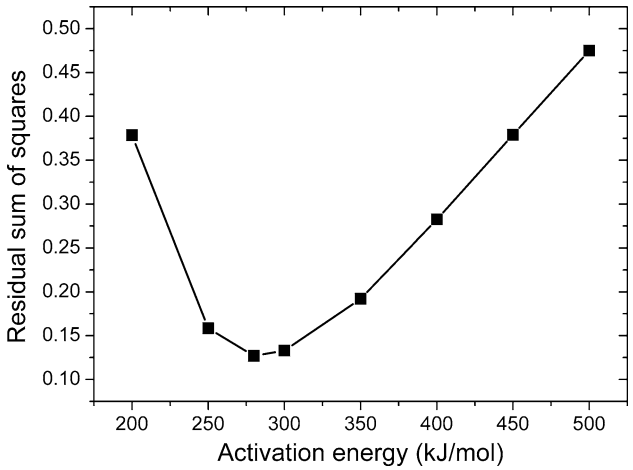

Fig. 3 Residual sum of squares as function of the tested activation energy

energy was obtained by fitting a Boltzmann sigmoidal curve to the set of experimental points:

$$\rho = A_1 + \frac{A_1 - A_2}{1 + \exp\left(\frac{\log(\Theta) - x_0}{d_x}\right)} \quad (6)$$

with A_1, A_2, x_0, and d_x numerical constants. As an alternative, the classical sigmoidal function [3] was also tested and gave exactly the same result for the activation energy. As shown in Fig. 3, the residual sum of the square deviations between experimental data points and fitting curve meets a minimum undoubtedly for a global activation energy value of 290 kJ/mol.

In the case of submicron alumina (and more generally electrically insulating powders), the densification mechanism was found to be the same during FAST as in HP, i.e., grain boundary diffusion [18]. For that, a rigorous methodology based on the use of the same processing parameters (powder, heating schedule, pressure, and atmosphere) and thorough measurement calibration was developed. No effect of electric field could be highlighted, and activation energies were found to be equal. Differences in densification curves were attributed to differences in real temperatures seen by the specimens. The value of activation energy measured from isothermal measurements lies typically in the range of 420–480 kJ/mol [17, 18]. An and Johnson [11] used an activation energy for pure fine alumina powder of 477 kJ/mol for their study case of HP, which showed an excellent agreement. Therefore, the lower value found in the present study needs to be rationalized. By coincidence, it corresponds to literature values of the activation energy for surface diffusion (230–280 kJ/mol [9]), which is a nondensifying mechanism. However, contrasting values resulting from different constant heating rates experiments have been very recently obtained, all on TMDAR alumina [9, 20, 21]. Depending on the processing method for the

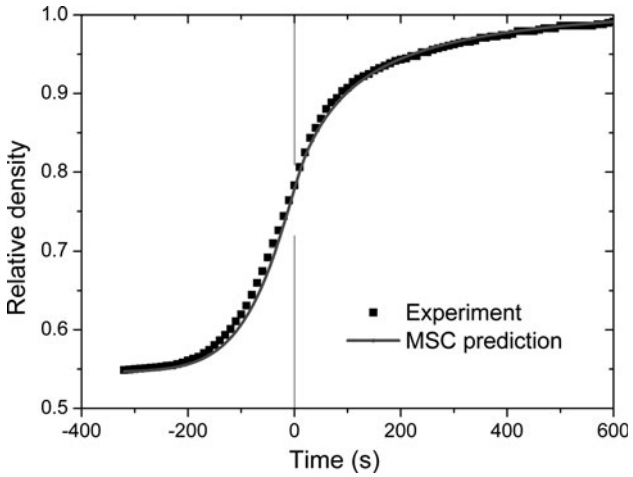

Fig. 4 Prediction with an activation energy of 290 kJ/mol and experimental curve for a heating rate of 75 K/min (from 800 to 1200 °C, under a constant applied stress of 50 MPa). Time origin represents the beginning of the isothermal step

sample shaping as well as the heating rate, different activation energies characterizing pressureless sintering were measured. On the one hand, specimens sintered by dry pressing and pressure filtration showed different apparent activation energies (700 and 605 kJ/mol, respectively), both higher than expected [20]. The analysis included heating rates between 5 and 25 K/min. On the other hand, very low-heating rates below 2 K/min lead to an enhanced neck growth due to surface diffusion during heating, which in turn seems to give high values of $\sim$1000 kJ/mol [21]. In contrast, higher heating rates may lead to temperature gradients in the densifying specimen. Motivated by FEM simulations of the temperature distribution, Raether et al. [9] proposed that too high heating rates (for example 25 K/min in their case) may lead to temperature heterogeneity within the specimen and consequently to artificially lowered activation energy values. When using FAST, it is clear that temperature gradients are expected at the high heating rates available. Temperature measurement, control, overheating are critical issues with this technique and a specimen heated at 1000 °C/min will meet entirely the required isothermal temperature only after a few minutes, and larger specimens will experience larger gradients. It was already shown that with a heating rate of 10 K/min, the temperature within the sample becomes homogeneous only after 60 s [18]. On the other hand, Olevsky et al. [22] have shown that high heating rates are expected to enhance the densification rates by leaving more quickly the temperature regime for which surface diffusion is dominant and avoiding too early pore spheroidization. These findings coincide with the lower value of the activation energy characterizing the whole sintering cycle measured here.

Apart from these considerations, the suitability of using MSC concept to FAST experiments is validated by predicting the densification curve at a rate of 75 K/min, which fits very well to the experimental curve, as presented in Fig. 4. However, the MSC as simple empirical approach to predict densification behavior has some limitations (i.e., a unique sintering path as function of density is prescribed) which constrains the flexibility of the modeling. This limits the possibilities for process optimization (for example, reaching the highest possible relative density with the smallest possible grain size), which is one of potentially achievable goals in spark-plasma sintering/FAST.

Conclusion

In this study, we have shown that the MSC approach can be applied to the Field-Assisted Sintering Technique (as well as HP, but with reduced range of heating rates). This complements other modeling methodologies like finite element simulations as proposed by Maizza et al. [23]. Experimental data confirm the general applicability of this theoretical framework and gives an apparent activation energy of $\sim$290 kJ/mol. As alumina densifies by grain boundary diffusion in the present conditions, this low value of the apparent activation energy might be due to thermal gradients in the specimens induced by rapid heating. However, even for the wide range of heating rates investigated, it seems that the temperature measurement and homogeneity within the specimen is still good enough to be described by the MSC framework. If relevant, other densification mechanisms could be implemented in the model in order to adequately describe the densification behavior of electrically conductive materials induced by the electric field or current.

Acknowledgements This work was financially supported by the Deutsche Forschungsgemeinschaft (Emmy Noether Program GU993-1/1). Michael Hoffmann is acknowledged for providing access to his FAST setup.

References

1. Su H, Johnson DL (1996) J Am Ceram Soc 79(12):3211
2. Hansen J, Rusin RP, Teng M, Johnson DL (1992) J Am Ceram Soc 75:1129
3. Johnson DL (2003) In: Messing G (ed) International conference on the science, technology, application of sintering, Pennsylvania, USA, pp. 15–17
4. Kiani S, Pan J, Yeomans JA (2006) J Am Ceram Soc 89(11):3393
5. Ewsuk KG, Ellerby DT, Diantanio CB (2006) J Am Ceram Soc 89(6):2003
6. Blaine DC, Gurosik JD, Park SJ, Heaney DF, German RM (2006) Metall Mater Trans 37A(3):715

7. Mazaheri M, Simchi A, Dourandish M, Golestani-Fard F (2009) Ceram Int 35:547
8. Hillman SH, German RM (1992) J Mater Sci 27:2641
9. Raether F, Schulze Horn P (2009) J Eur Ceram Soc 29:2225
10. Park SJ, Suri P, Olevsky E, German RM (2009) J Am Ceram Soc 92(7):1410
11. An K, Johnson DL (2002) J Mater Sci 37:4555
12. Munir ZA, Anselmi-Tamburini U, Ohyanagi M (2006) J Mater Sci 41:763. doi:10.1007/s10853-006-6555-2
13. Chaim R, Shen ZJ (2008) J Mater Sci 43:5023. doi:10.1007/s10853-008-2742-7
14. Frage N, Cohen S, Meir S, Kalabukhov S, Dariel MP (2007) J Mater Sci 42:3273. doi:10.1007/s10853-007-1672-0
15. Zeng H, Kuang CJ, Zhang JX, Yue M (2009) J Mater Sci 44:5509. doi:10.1007/s10853-009-3769-0
16. Coble RL, Ellis JS (1963) J Am Ceram Soc 46(9):438
17. Rahaman NM. (2003) Ceramic processing and sintering. Marcel Dekker Inc, New York
18. Langer J, Hoffmann MJ, Guillon O (2009) Acta Mater 57:5454
19. Zuo R, Rödel J (2004) Acta Mater 52:3059
20. Aminzare M, Golestani-Fard F, Guillon O, Mazaheri M, Rezaie HR, Mater Sci Eng A. doi:10.1016/j.msea.2010.03.051
21. Bernard-Granger G, Guizard C, Addad A (2007) J Mater Sci 42:6316. doi:10.1007/s10853-006-1206-1
22. Olevsky EA, Kandukuri S, Froyen L (2007) J Appl Phys 102:114913
23. Maizza G, Grasso S, Sakka Y (2009) J Mater Sci 44:1219. doi:10.1007/s10853-008-3179-8